

RESEARCH

Open Access



NHH promotes Sepsis-associated Encephalopathy with the expression of AQP4 in astrocytes through the gut-brain Axis

Lina Zhao¹, Zhen Zhang¹, Pei Wang¹, Nannan Zhang¹, Hao shen¹, Hening Wu¹, Zhiyong Wei¹, Fei Yang², Yuning Wang², Zhijie Yu², Haibo Li³, Zhanfei Hu³, Hongyan Zhai⁴, Zhiwei Wang¹, Fuhong Su⁵, Keliang Xie^{1,6*} and Yun Li^{6*}

Abstract

Sepsis-associated encephalopathy (SAE) is a significant cause of mortality in patients with sepsis. Despite extensive research, its exact cause remains unclear. Our previous research indicated a relationship between non-hepatic hyperammonemia (NHH) and SAE. This study aimed to investigate the relationship between NHH and SAE and the potential mechanisms causing cognitive impairment. In the *in vivo* experimental results, there were no significant abnormalities in the livers of mice with moderate cecal ligation and perforation (CLP); however, ammonia levels were elevated in the hippocampal tissue and serum. The ELISA study suggest that fecal microbiota transplantation in CLP mice can reduce ammonia levels. Reduction in ammonia levels improved cognitive dysfunction and neurological impairment in CLP mice through behavioral, neuroimaging, and molecular biology studies. Further studies have shown that ammonia enters the brain to regulate the expression of aquaporins-4 (AQP4) in astrocytes, which may be the mechanism underlying brain dysfunction in CLP mice. The results of the *in vitro* experiments showed that ammonia up-regulated AQP4 expression in astrocytes, resulting in astrocyte damage. The results of this study suggest that ammonia up-regulates astrocyte AQP4 expression through the gut-brain axis, which may be a potential mechanism for the occurrence of SAE.

Summary

This study elucidates the intricate relationship between gut microbiota, ammonia production, and brain dysfunction in sepsis associated encephalopathy.

Keywords Sepsis-associated encephalopathy, AQP4, GFAP, Gut-brain axis, Astrocyte

*Corresponding author: Keliang Xie and Yun Li.

*Correspondence:

Keliang Xie
xiekeliang2009@hotmail.com
Yun Li

cfsyy_liyun@126.com

¹Department of Critical Care Medicine, Tianjin Medical University General Hospital, Tianjin 300052, China

²Department of Critical Care Medicine, Chifeng Municipal Hospital, Chifeng Clinical Medical College of Inner Mongolia Medical University, Chifeng 024000, China

³Department of Anesthesiology, Chifeng Municipal Hospital, Chifeng Clinical Medical College of Inner Mongolia Medical University, Chifeng 024000, China

⁴Department of Ultrasound, Tianjin Medical University General Hospital, Tianjin 300052, China

⁵Experimental Laboratory of the Department of Intensive Care, Erasme Hospital, Université Libre de Bruxelles, Brussels 1070, Belgium

⁶Department of Anesthesiology, Tianjin Institute of Anesthesiology, Tianjin Medical University General Hospital, Tianjin 300052, China



Introduction

Sepsis-associated encephalopathy (SAE) is a major cause of both short- and long-term mortality in patients with sepsis. Its incidence and mortality rates are increasing globally, posing a serious threat to public health that urgently needs to be solved [1–3]. SAE manifests as cognitive dysfunction and changes in the levels of consciousness and behavior [3]. Although inflammation, mitochondrial dysfunction, and microglial cell activation have been reported as potential mechanisms of SAE, the exact pathogenesis remains unclear, and effective prevention and intervention measures are still lacking.

Ammonia serves as a crucial neurotoxin, playing a significant role in hepatic encephalopathy [4]. Hyperammonemia, stemming from non-hepatic conditions, is increasingly documented among critically ill patients, notably those afflicted by sepsis [5–7]. Our previous investigations have revealed a correlation between non-hepatic hyperammonemia (NHH) and sepsis-associated encephalopathy (SAE). The etiology of NHH in septic patients may stem from factors such as heightened ammonia generation within the intestine and amplified breakdown of amino acids [8, 9]. The gastrointestinal tract, a vital component of the immune system, is susceptible to injury following sepsis, particularly in instances of septic shock. Subsequent to intestinal damage, dysbiosis in the gut microbiota is prone to occur [10]. Ammonia is generated from amino acids in response to intestinal bacteria; Therefore, the disruption of the gut microbiota and the upgrading of amino acid metabolism after sepsis may contribute to NHH production.

Astrocyte edema stands as a pivotal mechanism contributing to the onset of sepsis-associated encephalopathy (SAE) alongside neuronal damage [11]. Additionally, astrocytes play a crucial role in the development of hepatic encephalopathy induced by ammonia [12]. Aquaporin 4 (AQP4) is a specialized membrane-bound channel highly expressed in astrocytes, governing water movement in and out of these cells. Moreover, AQP4 activation elevates astrocyte activity through increased AQP4 expression [11, 13]. Given its significance in astrocytic function, AQP4 emerges as a key player in astrocytic injury. Given its importance in astrocyte function, the study have found AQP4 to be a key player in ammonia-induced astrocyte injury in hepatic encephalopathy [12]. However, it is unclear whether they are involved in the occurrence of SAE.

This study aimed to explore the origins of ammonia in a mouse model of cecal ligation and puncture (CLP) by examining the potential increase in ammonia-producing bacteria in the intestine, utilizing 16 S rDNA sequencing and metabolomics technology. Pathophysiological alterations and the underlying mechanisms of ammonia-induced brain injury in a CLP mouse model were

investigated at both animal and cellular levels. This was achieved through fecal microbiota transplantation and a comprehensive array of analyses including morphological, functional, molecular biology, and neuroimaging techniques (refer to Fig. 1).

Results

Elevated levels of NHH in serum and hippocampal tissues of CLP mice

Our previous studies found that patients with sepsis and normal liver function had elevated ammonia levels and that the serum ammonia level correlated with impaired consciousness [14]. We speculate that non-hepatic hyperammonemia (NHH) may be a potential mechanism underlying SAE [9]. To verify the change in ammonia in SAE, we used CLP surgery to evaluate the mice's response to SAE to avoid liver damage, in this study, a moderate CLP model was used [15]. In this study, the mortality rate of moderate CLP model mice was 48%. We also evaluated HE staining and measured alanine aminotransferase ($p < 0.01$), glutamate aminotransferase ($p < 0.01$), and total bilirubin ($p > 0.05$) levels in the livers of the three groups ($n = 6$) at 24 h, 48 h, and 72 h after CLP (Fig. 2a and b). In three groups, CLP resulted in mildly abnormal liver function; however, the hepatocytes of the rats were arranged neatly, the hepatic lobule structure was intact, and there were no significant abnormalities in the liver function indices of the three groups (Fig. 2b). However, serum ($p < 0.01$) and hippocampal ($p < 0.001$) ammonia levels in the CLP group were significantly higher than those in the control and sham groups (Fig. 2c).

Fecal microbial transplantation in CLP mice can reduce ammonia levels and may be associated with *bacilli*

Increased abundance of *bacilli* in CLP mice

After the CLP model was established, the fecal microorganisms of the mice in the control group were transplanted into the CLP mice for 3 consecutive days. HE staining was used to observe the morphological changes in the ileum and intestinal pH test in the three groups of mice ($n = 6$). After CLP, the ileum villus length and crypt depth were decreased, and pH was increased compared to the control and sham groups ($p < 0.0001$ or $p < 0.01$) (Fig. 3a and b). CLP disrupts the intestinal structure of mice and pH. After fecal microbe transplantation (FMT), the feces of mice in each group ($n = 6$) were collected, and 16 S rDNA sequencing technology was used to observe the changes in microbial species and abundance in each group. After CLP, at the class level, the most abundant microbes of *Bacteroidia* decreased, while *Bacilli* increased compared to the control group and sham group. After FMT, the abundance of *Bacteroidia* microbes increased, and *Bacilli* decreased in the community plot ($p < 0.05$) (Fig. 3c). The diversity of the

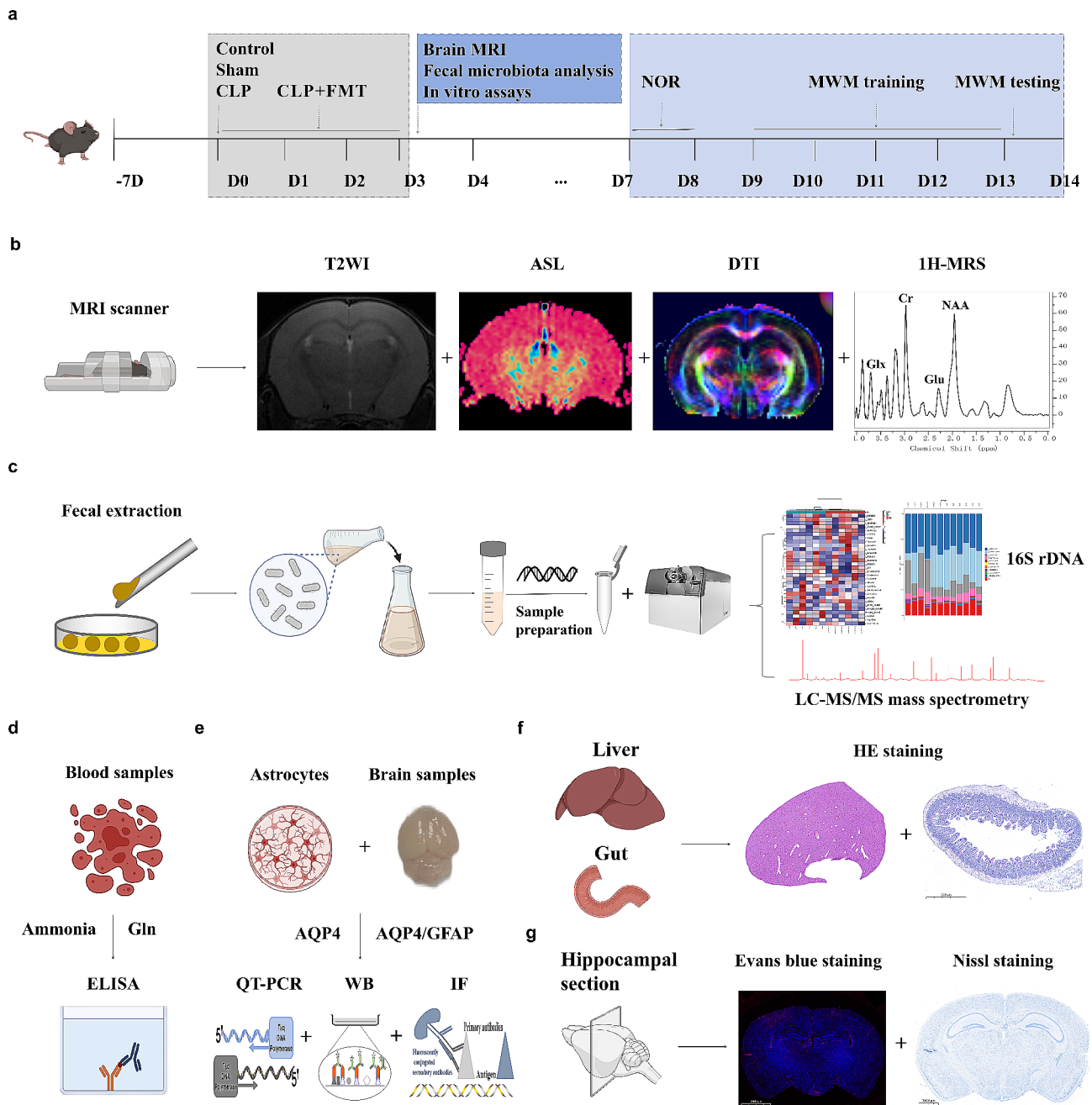


Fig. 1 Experimental flow chart. The mice were allowed to acclimatize to the experimental environment for 1 week before the start of the experiment. After CLP or sham surgery in C57BL6/J mice, CLP mice were transplanted with fecal bacteria from the control group mice for 3 consecutive days. **(a)** On the 3 days, the species and abundance of intestinal microbiota were detected (16 S rDNA), neuroimaging **(b)**, mettabomics **(c)**, including T-2 weighting, DTI, ASL, 1 H-MRS, and molecular biology tests including ELISA **(d)**, Western Blot, QT-PCR, immunofluorescence **(e)**, HE staining **(f)**, Nissl staining and Evans blue staining **(g)**. CLP: cecal ligation and perforation; ASL: Arterial spin labeling; DTI: Diffusion Tensor Imaging; 1 H-MRS: proton magnetic resonance spectroscopy; T2WI: T2-weighted imaging; WB: Western Blot. * $p < 0.05$, ** $p < 0.01$, *** $p < 0.001$, **** $p < 0.0001$

microbiota was significantly lower in the CLP group than in the control and sham groups, as determined by the Chao1 index ($p < 0.05$); however, there were no significant differences in the Shannon and Simpson indices (Fig. 3d). Additionally, the analysis of microbiome beta diversity using Unweighted Unifrac and principal

coordinate analysis (PCoA) indicated significant differences in community components between the CLP group and the other three groups, indicating that CLP affected gut microbiota composition ($p < 0.01$) (Fig. 3e and f). The LDA effect size (LEfSe) analysis showed that the key bacteria in the sham group were *Bacteroidales*,

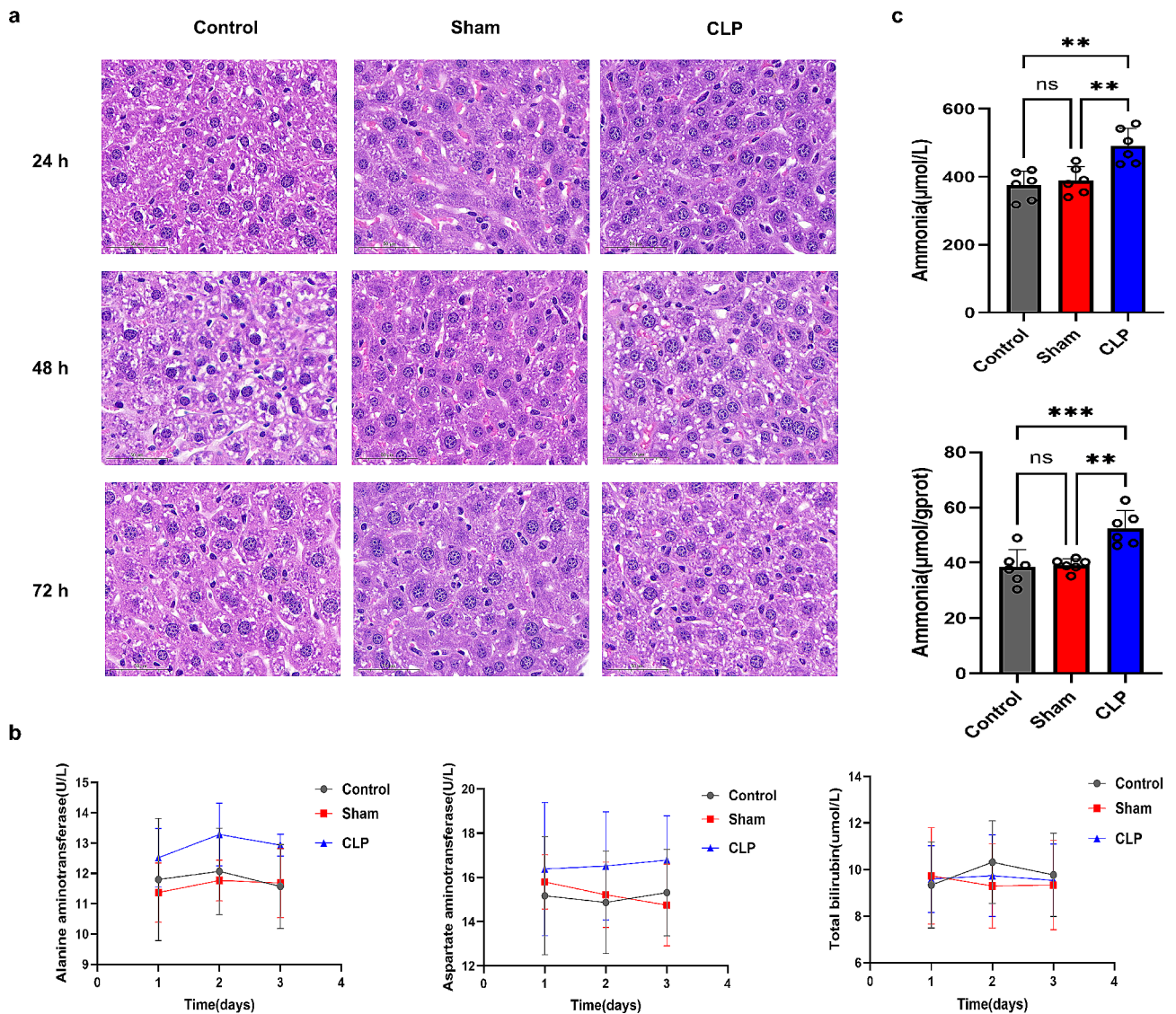


Fig. 2 Assessing liver function after mild CLP model in three groups of mice. **(a)** : HE staining of the liver at 24 h, 48 h, 72 h after CLP in the three groups. In the three groups, the hepatocytes of the rats were arranged neatly, and the hepatic lobule structure was intact. **(b)** : CLP caused a slight increase in alanine aminotransferase and aspartate aminotransferase, but the total bilirubin level did not change significantly at 24 h, 48 h, 72 h after CLP. **(c)** : Ammonia levels in serum and hippocampal tissues were significantly higher in the CLP group than in the control and sham groups. * $p < 0.05$, ** $p < 0.01$, *** $p < 0.001$, **** $p < 0.0001$

Muribaculaceae, *Erysipelotrichaceae*, *Allobaculum*, *Prevotellaceae*, and *Alloprevotella*. The key bacteria in CLP mice were *Bacilli*, *Clostridium*, *Firmicutes*, *Lactobacillales*, *Enterobacteriales*, *Streptococcus*, and *Enterococcus* were predominant (Fig. 3g and Supplementary Materials 1). Fecal transplantation resulted in decreased relative abundance of *Bacilli* and *Clostridium* and increased relative abundance of *Rhodospirillales*, *Moraxellaceae*, *Clostridia_vadinBB60_group*, *Gastranaerophilales*, and *Clostridia_UCG_014* in CLP group (Fig. 3h and Supplementary Materials 2). These results showed that CLP significantly altered the type and abundance of the intestinal flora.

Functional annotation and differential analyses were conducted to investigate the effects of modified gut microbiota. The Kyoto Encyclopedia of Genes and Genomes (KEGG) and Gene Ontology (GO) functional annotation results showed that the relative abundance values of amino acid metabolism in the CLP group were higher than those in the other groups (Fig. 3i). Functional difference analysis also showed that “Carbohydrate metabolism,” “Amino acid metabolism,” “Metabolism of other amino acids,” and “Infectious disease: bacterial” were stimulated in the CLP group (Fig. 3j) ($p < 0.05$) after FMT, they were suppressed (Fig. 3k) ($p < 0.05$). Principal Component Analysis (PCA) analysis of microbiota

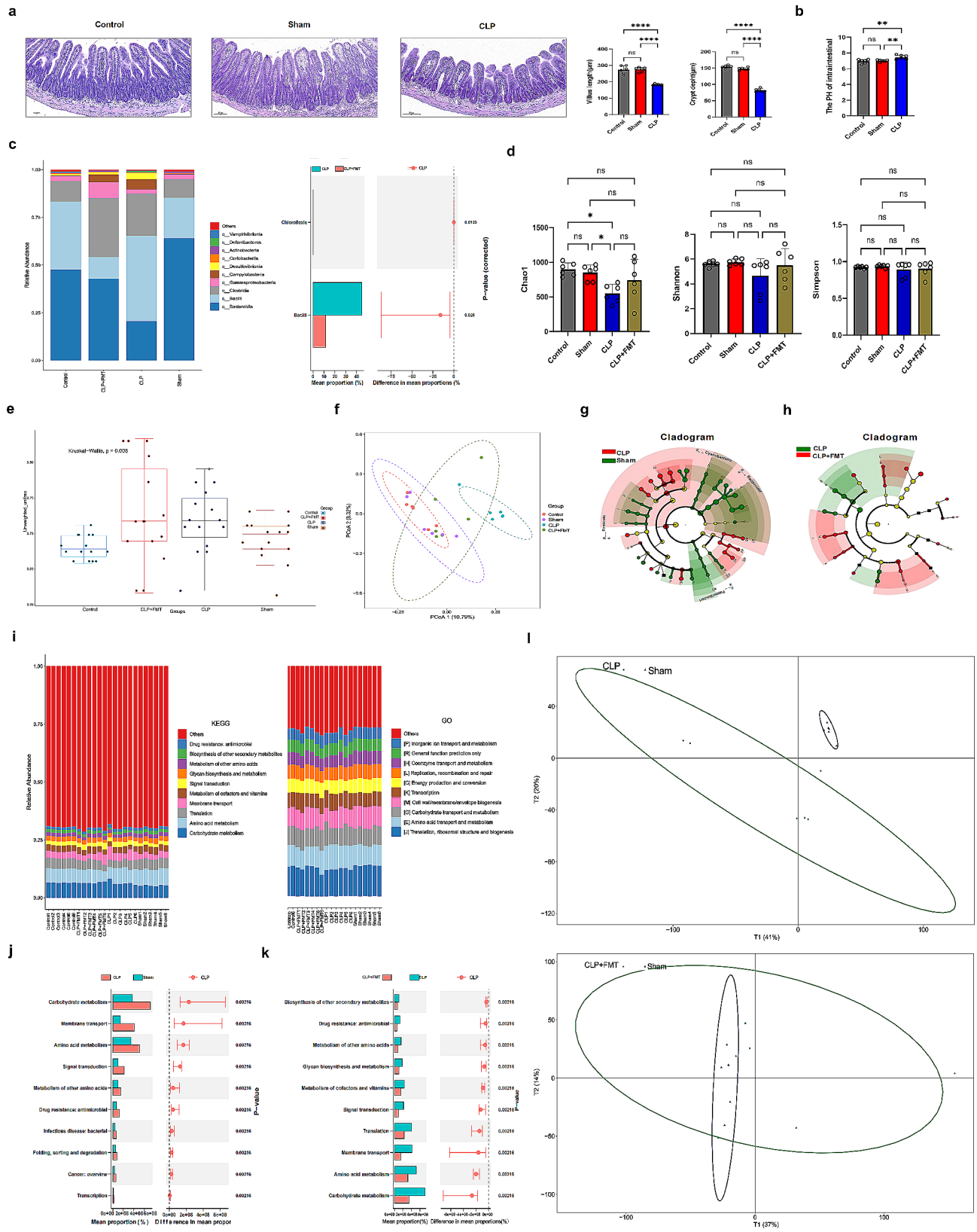


Fig. 3 (See legend on next page.)

(See figure on previous page.)

Fig. 3 Fecal microbial transplantation in CLP mice can reduce ammonia levels and may be associated with *Bacilli*. **(a)**: HE staining was used to observe the morphological changes of the ileum. **(b)**: Intestinal pH test in the three groups of mice. **(c)**: Observe the changes in microbial species and abundance in each group at the class level through 16 S rDNA technology. **(d)**: Comparison of microbial α diversity among groups. **(e)** and **(f)**: Comparison of microbial β diversity among groups. **(g)**: LDA effect size (LEfSe) analysis CLP group compared with sham group. **(h)**: LEfSe analysis CLP group compared with (CLP + FMT) group. **(i)**: The functional annotation and differential analyses by KEGG and Go. **(j)** and **(k)**: Functional difference was analyzed for each group. Figure 3: PCA analysis of microbiota function. KEGG: The Kyoto Encyclopedia of Genes and Genomes; GO: the Gene Ontology. * $p < 0.05$, ** $p < 0.01$, *** $p < 0.001$, **** $p < 0.0001$

function showed that there was a significant difference in microbiota function between the CLP and sham groups, and microbiota function was similar after FMT (Fig. 3l). Therefore, it is speculated that amino acid levels may be related to changes in the intestinal flora.

FMT reduced amino acid metabolism and ammonia levels in CLP mice

Metabolomic analysis by LC-MS/MS showed that amino acids accounted for 55% of all identified metabolites (Fig. 4a). The amino acid levels in the CLP group were significantly higher than those in the sham group, with Log2FC values ranging from 1.15 to 60.87 in volcano plots ($p < 0.05$). The identified amino acids included 5-Aminolevulinic acid, 5-Hydroxylysine, Alloisoleucine, Alpha-aminobutyric acid, Arginine, Asparagine, Glutamine, Histidine, Homoserine, Lysine, Methionine, N-Acetylalanine, Phenylalanine, Proline, Serine, Threonine, Tryptophan, Tyrosine, and Valine (Fig. 4b). After FMT, the amino acid substance of the CLP group was significantly reduced, with Log2FC values ranging from 0.10 to 0.49 ($p < 0.05$), the reduced of amino acids included Arginine, Asparagine, Creatine, Glutamine, Homoserine, N-acetylalanine, Serine, and Threonine (Fig. 4c). Additionally, the chord diagrams the four groups further confirmed that there was a significant difference in amino acid levels ($p < 0.05$), with a correlation between amino acids ($r > 0.8$) (Fig. 4d, Supplementary material 3). KEGG pathway analysis of metabolites showed that amino acid metabolism increased after CLP, and the difference in abundance was higher than that of the sham group, including phenylalanine, tyrosine, and tryptophan biosynthesis; glycine, serine, and threonine metabolism after Fecal microbial transplantation, arginine, and proline metabolism; and glycine, serine, and threonine metabolism were reduced (Fig. 4e). Additionally, after FMT in CLP mice, ammonia levels in the serum and hippocampal tissues decreased (Fig. 5d). These results showed that FMT reduced amino acid metabolism and ammonia levels in the CLP group. Amino acid metabolism is the primary source of ammonia.

Bacilli has a significant correlation with amino acid metabolism and ammonia

In this study, the association between intestinal microbes and metabolic products was analyzed in each group. The *Bacilli* of CLP group and Sham group differentiating

bacteria is positively correlated with the metabolism of Arginine, Asparagine, Cysteine, Glutamine, Glycylleucine, Histidine, Homoserine, Isoleucine, Lysine, N-Acetylalanine, N-acetyltryptophan, Norleucine, Phenylalanine, Proline, Serine, Tyrosine, and Threonine. The *Bacilli* of CLP and Sham group differentiating bacteria is positively correlated with the metabolism of Arginine, Asparagine, Creatine, Creatinine, Glutamine, Homoserine, N-Acetylalanine, Serine, Threonine (Fig. 4f). Therefore, we speculate that the increase in *Bacilli* after CLP may be related to the occurrence of NHH.

Decreased ammonia levels improved cognitive dysfunction and neuronal damage in CLP mice Neuroimaging

T2-weighted Arterial spin labeling (ASL), Diffusion Tensor Imaging (DTI), and Proton magnetic resonance spectroscopy (1 H-MRS) were performed 72 h after CLP surgery ($n = 6$). T2-weighted test results showed that the signal intensity of the CLP group was significantly higher than that of the sham and control groups, which showed an increase in water content in mouse brain tissue after CLP. Furthermore, FMT reduced ammonia levels, resulting in decreased water content of brain tissue in CLP mice ($p < 0.001$ or $p < 0.05$). ASL examination results showed a significant decrease in blood flow in the hippocampal region of CLP mice. After FMT in CLP mice, cerebral blood flow improved ($p < 0.01$ or $p < 0.05$ or $p < 0.0001$). DTI test results showed that the fractional anisotropy (FA) and Axial Diffusion (AD) of hippocampal tissues in CLP mice were significantly higher than those in the sham and control groups, while the Radical Diffusion (RD) and Mean Diffusivity (MD) of hippocampal tissues in CLP mice were significantly lower than those in the sham and control groups ($p < 0.01$, $p < 0.05$, or $p < 0.0001$), suggesting that CLP could lead to impaired nerve fiber integrity in mice, with improved nerve fiber integrity observed after reducing ammonia level (Fig. 5a). Imaging studies have shown that CLP can lead to cerebral edema, decreased cerebral blood flow, and destruction of the nerve fiber bundle integrity. However, after FMT and reduction of ammonia levels in mice, cerebral edema, decreased cerebral blood flow, and nerve fiber incompleteness improved.

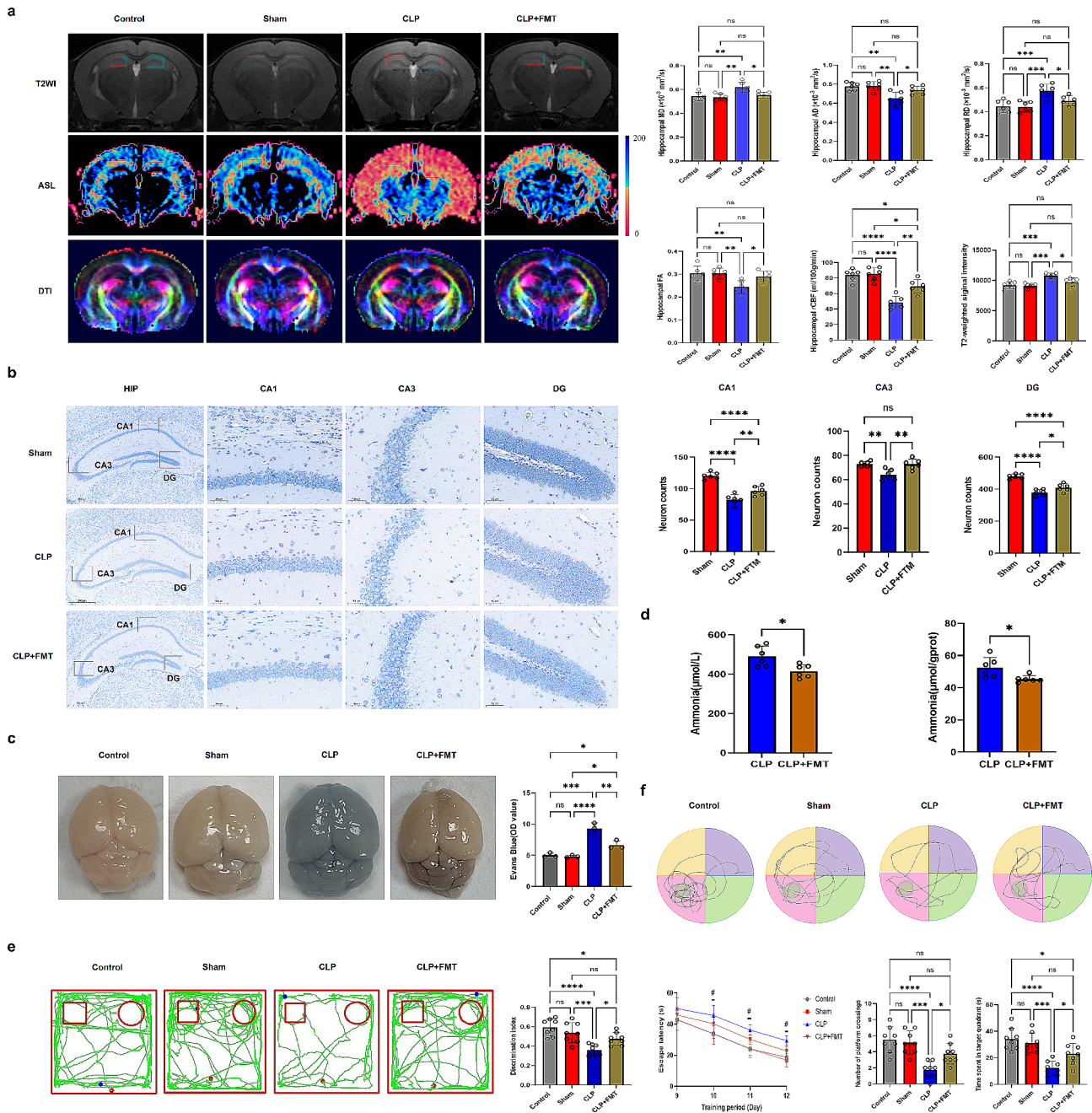


Fig. 5 The decrease in ammonia levels improved cognitive dysfunction and neuronal damage in CLP mice. **(a)**: T2WI, ASL, and DTI were performed for 72 h after CLP surgery in each group. The red box shows the comparison of T2WI signal density and hippocampal rCBF. **(b)**: The Nissl staining of hippocampal tissues (DG, CA1, CA3) was performed in each group. **(c)**: Evans blue dye extravasation was used to assess changes in vascular permeability in each group. **(d)**: Ammonia levels in the hippocampus and serum were compared between the CLP group and the CLP + FMT group. **(e)**: The novel object recognition was completed in each group of mice. **(f)**: The Morris Water Maze was completed in each group of mice. T2WI: T2-weighted imaging * $p < 0.05$, ** $p < 0.01$, *** $p < 0.001$, **** $p < 0.0001$

Nissl staining of hippocampal tissues

Nissl staining of hippocampal tissues was performed 72 h after CLP surgery ($n=6$). The results showed that CLP can lead to a decrease in hippocampal neuronal cells. Moreover, after reducing ammonia levels, the damage

caused by CLP to neuronal cells was mitigated ($p < 0.01$, $p < 0.05$, and $p < 0.0001$, respectively) (Fig. 5b).

Blood-brain barrier permeability

Evans blue dye extravasation was used to evaluate alterations in vascular permeability 72 h after CLP ($n=6$).

Evans blue extravasation into the entire brain was measured in the CLP group. The large increase in Evans blue extravasation in the CLP mice was significantly reduced in the CLP+FMT mice (Fig. 5c). Pathological studies have shown that CLP not only damages neuronal cells but also destroys the blood-brain barrier and reduces brain damage caused by CLP after reducing ammonia levels ($p < 0.01$, $p < 0.05$, and $p < 0.0001$).

Behavioral

On days 7 and 8 after CLP [35], new-object recognition was evaluated for cognitive memory in each mouse group ($n=8$). The results showed a reduction in the discrimination index of mice after CLP, after FMT in the CLP group, the discrimination index improved ($p < 0.001$, $p < 0.05$, and $p < 0.0001$, respectively) (Fig. 5e). From days 9 to 13 after CLP, the Morris Water Maze was employed to evaluate the spatial learning and memory function of each group of mice. The number of platform crossings and the time spent in the target quadrant in the CLP group were significantly reduced compared to the sham group and the control group, while the escape latency was prolonged ($p < 0.001$, $p < 0.05$, and $p < 0.0001$, respectively) (Fig. 5f). The behavioral study results showed impaired cognitive function of mice after CLP, and the reduction of ammonia levels could improve the cognitive function of CLP mice, thereby further confirming the success of the SAE model.

Ammonia up-regulates astrocytes AQP4 may be the mechanism of SAE

The western blot (WB) analysis ($n=6$) and Quantitative Real-time PCR (QT-PCR) ($n=6$), immunofluorescence staining ($n=6$) results showed that 72 h after CLP, the expression of AQP4 and Glial fibrillary acidic protein (GFAP) proteins and genes, as well as the number of GFAP-positive cells, and the positive rate of AQP4 cell number as a proportion of GFAP cell number in hippocampal tissues were significantly increased ($p < 0.0001$ or $p < 0.001$ or $p < 0.01$ or $p < 0.05$) (Fig. 6a, b and c). Additionally, 1 H- MRS study found that after CLP, the levels of glutamate(Glu)/creatine(Cr) and N-acetyl aspartate(NAA)/Cr in the hippocampus of mice were decreased, indicating neuronal damage, while the level of Glx (glutamate+glutamine)/Cr was increased. After FMT, the serum ammonia level was decreased, neuronal damage was improved, and the level of Glx/Cr was decreased ($p < 0.0001$ or $p < 0.001$ or $p < 0.01$ or $p < 0.05$) (Fig. 6d). Simultaneously, the use of the Elisa method to detect glutamine levels in serum and hippocampal tissues of mice in each group was consistent with the results of 1 H-MRS (Fig. 6e). A previous study had found that ammonia enters the brain and binds to GLU to produce glutamine, further activating astrocytic AQP4 expression

and leading to brain damage [16]. To further verify the mechanism of action of ammonia in the brains of CLP-treated mice, cellular experiments were performed.

Ammonia up-regulates astrocytes' AQP4 expression by activating astrocytes, resulting in astrocytes damage

Astrocytes were treated with NH_4Cl for 72 h ($n=3$) to test the effect of ammonia on them. Immunofluorescence results showed that astrocytes were activated, and the number of GFAP-positive cells increased significantly compared to the control group (Fig. 7a). Subsequently, the number of AQP4 and GFAP co-expressed cells also increased (Fig. 7a) ($p < 0.0001$ or $p < 0.001$ or $p < 0.01$). Additionally, compared with the control group, astrocyte viability decreased after NH_4Cl treatment (Fig. 7d). WB and QT-PCR results showed that the expression levels of AQP4 protein and gene increased after NH_4Cl stimulation ($p < 0.0001$, $p < 0.001$, $p < 0.01$, and $p < 0.05$, respectively) (Fig. 7b and c). To further demonstrate the effect of AQP4 on astrocytes, we treated astrocytes with the AQP4 inhibitor TGN20, which showed decreased astrocyte activation levels, decreased GFAP-positive cell numbers, decreased levels of co-expression with AQP4, and increased astrocyte viability (Fig. 7a and d). Therefore, cell experiments confirmed that ammonia can induce an increase in AQP4 expression and activate astrocytes.

Discussion

The incidence of NHH is as high as 76% in critically ill patients [17]. Particularly, it has a high incidence among patients with sepsis in critical care settings [6, 8, 18]. In this study, NHH also occurred in the acute phase of CLP in mice, and the results were consistent with those observed in patients with sepsis. Ammonia is primarily produced by the urease generated by intestinal bacteria, serving as the main source of serum ammonia.

After sepsis, the intestinal barrier becomes susceptible to damage, and such damage can contribute to the progression of sepsis [19, 20]. Consistent with these findings, in this study, the ileum villus length and crypt depth were decreased, and pH was increased after CLP, indicating disruption of the intestinal structure. Moreover, CLP led to intestinal dysbiosis, as evidenced by significant changes in the species and abundance of intestinal microbiota. Specifically, the Chao1 index and beta diversity in the CLP group were significantly different from those in the Sham group and the control group. The main manifestations included an increase in *Bacteroidia* and a decrease in *Bacilli*. The gut microbiota is closely related to changes in ammonia levels [21]. In this study, both the serum ammonia and brain tissue ammonia levels of the CLP group decreased after Fecal microbial transplantation, aimed at restoring the normal intestinal microbial state of the CLP group mice.

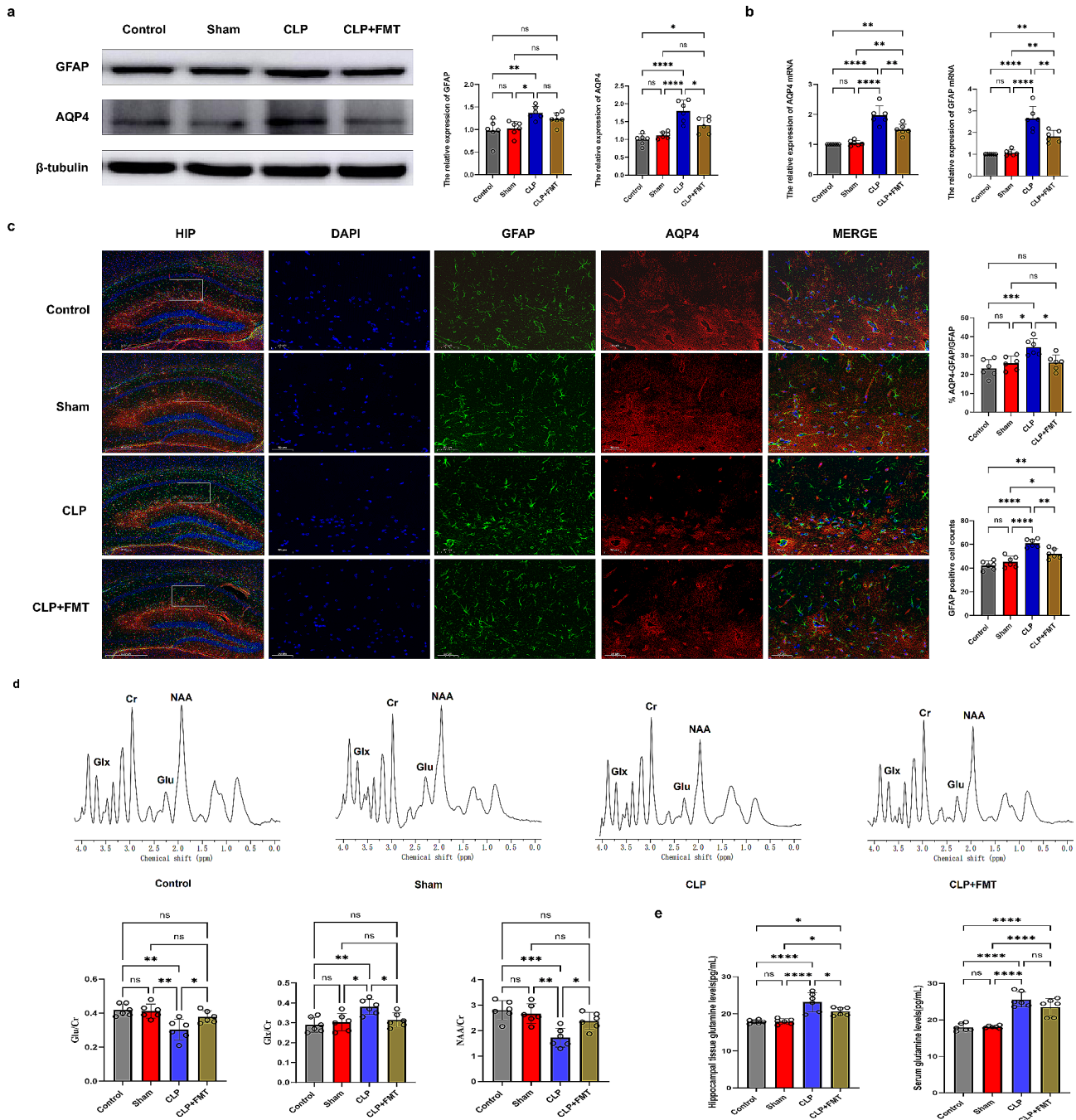


Fig. 6 Ammonia up-regulates astrocytes AQP4 may be the mechanism of SAE. (a) : The expression of AQP4 and GFAP protein in hippocampal tissue was detected by western blot. (b) : The expression of AQP4 and GFAP gene in hippocampal tissue was detected by QT-PCR. (c) : Hippocampal tissue AQP4 co-expression with GFAP was detected by immunofluorescence. (d) : The changes in the level of metabolites in the hippocampus of mice in each group were detected by 1 H-MRS. (e) : Comparison of glutamine levels in serum and hippocampal tissues of mice in each group. * $p < 0.05$, ** $p < 0.01$, *** $p < 0.001$, **** $p < 0.0001$

Metabolomic analysis by liquid chromatography-tandem mass spectrometry showed that the amino acid levels in the CLP group were significantly higher than those in the sham group. Moreover, the level of amino acid metabolism in the CLP group decreased after fecal transplantation. Enrichment and correlation analyses showed that

Bacilli regulate amino acid metabolism and are closely related. *Bacilli*, known as a representative urease-producing strain [22], promotes an increase in ammonia levels. Therefore, we hypothesize that the increase in NHH levels in CLP model mice is associated with the most significant change in the abundance of *Bacilli*. Based on

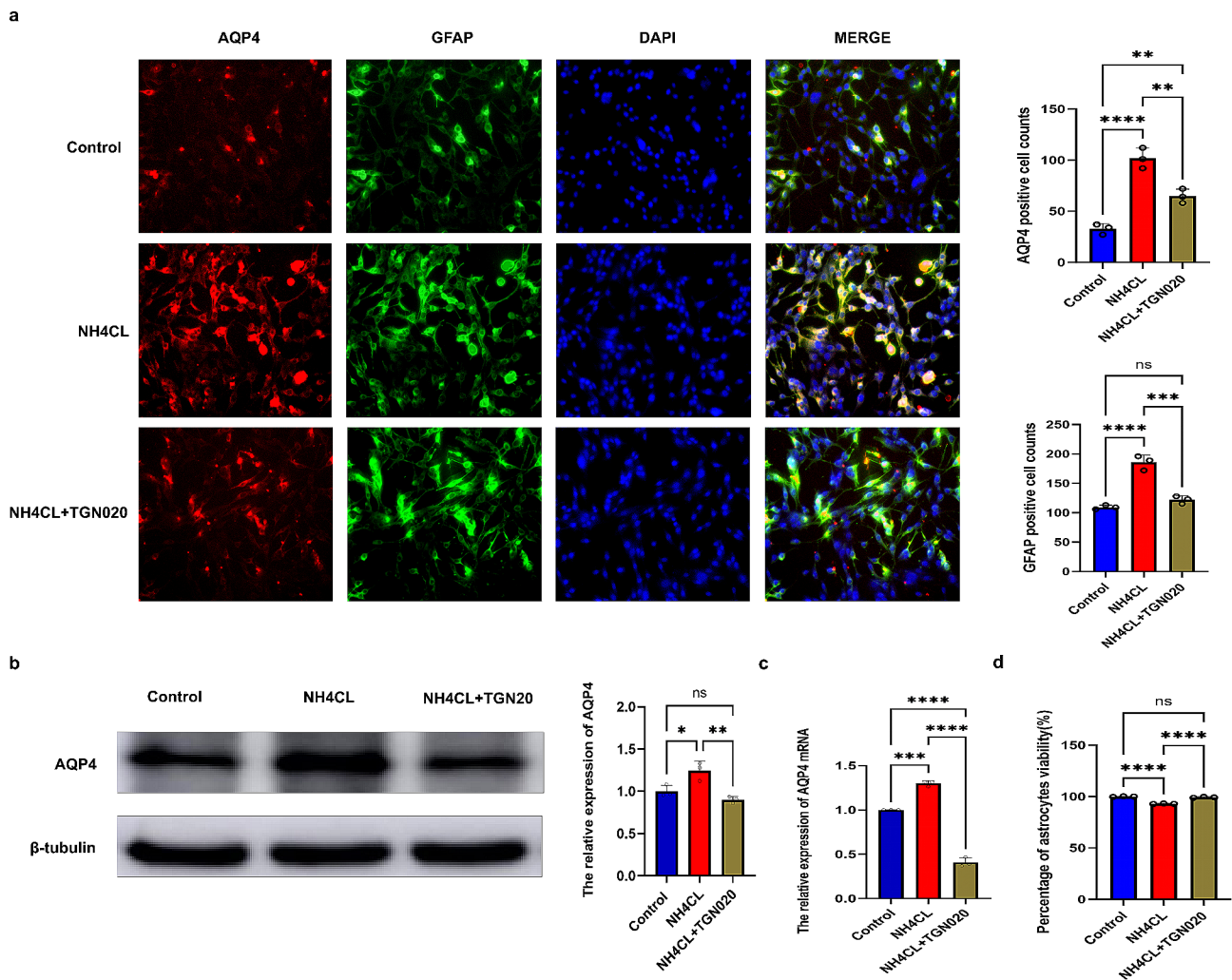


Fig. 7 Ammonia up-regulates astrocytes' AQP4 expression by activating astrocytes, resulting in astrocytes damage. **(a)** : Immunofluorescence co-expression of AQP4 and GFAP in astrocytes in each group. **(b)**: AQP4 protein expression in astrocytes was detected by western blot. **(c)** : AQP4 gene expression in astrocytes was detected by QT-PCR. **(d)**: Astrocyte viability was measured. * $p < 0.05$, ** $p < 0.01$, *** $p < 0.001$, **** $p < 0.0001$

the changes in amino acid levels observed in CLP mice model and after Fecal microbial transplantation, as well as the correlation analysis results between gut microbiota and metabolomics, we deduced that *Bacilli* regulate the increased metabolism of Arginine, Asparagine, Glutamine, Homoserine, N-Acetylalanine, Serine, and Threonine. These pathways represent potential mechanisms underlying the occurrence of NHH in CLP mice model.

Ammonia is an important neurotoxic substance, which is also an important mechanism for the occurrence of hepatic encephalopathy [4]. In recent years, the rise in ammonia levels unrelated to liver dysfunction has received increased attention due to its effect on the nervous system. Ammonia produced by the gut microbiome can help buffer stress in the host, thereby providing a gut-brain signaling basis for emotional behavior [21]. In this study, we observed increased ammonia levels in CLP model mice despite their normal liver function. However,

after Fecal microbial transplantation, ammonia levels were reduced in CLP model mice. This reduction was associated with improved cognitive function (MWM and NOR), cerebral edema (T2-weighted imaging, T2WI), cerebral ischemia (ASL), improvement of nerve fiber structural integrity (DTI), blood-brain barrier permeability (Evans blue), and increased neuronal cells in the hippocampus (Nissl staining). Therefore, NHH also plays an important role in brain injury in CLP mice based on multimodal brain evaluation in CLP mouse models. Several studies have shown that the gut-brain axis plays an important role in the pathogenesis of SAE, demonstrating that the gut microbiota facilitates SAE susceptibility [23, 24]. However, in the present study, we found that gut microbes increased ammonia levels by regulating amino acid metabolism, resulting in nervous system damage in SAE mice.

After ammonia enters the brain tissue, it is rapidly taken up by astrocytes and synthesized into glutamine by glutamine synthetase. The inhibition of astrocyte proliferation by ammonia is mediated by l-methionine sulfoximine, oxidative stress, and p38(MAPK) -MAPK-dependent activation of p53 in hepatic encephalopathy [25]. Additionally, the research has shown that ammonia causes neuronal disinhibition and seizures by disrupting astrocyte potassium buffering [26]. However, the mechanism of ammonia in SAE is still unclear. In this study, cerebral edema occurred in CLP mice in T2-weighted imaging images of CLP mouse models, and cerebral edema was reduced after reducing ammonia level expression. Astrocytic edema is an important mechanism of cerebral edema. AQP4 in astrocytes is the main protein controlling the inflow and outflow of water [27]. In this study, the expression of GFAP and AQP4 proteins and genes in CLP mouse models increased, indicating that astrocytes and aquaporin cells were activated in CLP mice. Additionally, the AQP4-GFAP/GFAP ratio in CLP mice was significantly increased, and GFAP and AQP4 were co-expressed. 1 H- MRI studies showed that after CLP, the levels of Glu/Cr and NAA/C in the brain of mice were decreased, indicating neuronal damage. Meanwhile, the levels of glutamine were increased. However, after reducing ammonia levels, the expression of GFAP and AQP4 proteins, genes, and cell counts of CLP mice decreased, and neuronal damage improved. Additionally, although there was no significant difference in glutamine levels, it was reduced in the serum and hippocampus. Based on these findings, we speculate that NHH induces

the upregulation of AQP4 expression in astrocytes, leading to astrocyte swelling, reduced cerebral blood flow, and neuronal damage, potentially contributing to the mechanism of brain injury in CLP mice (Fig. 8).

To further clarify the mechanism of NHH-induced brain injury in the mouse model of CLP, cell experiments were performed. The results showed that the number of GFAP and AQP4 co-expressing cells increased significantly after the NH₄Cl culture of astrocytes. Furthermore, GFAP expression was reduced when the AQP4 inhibitor TGN020 was added. These findings suggest that ammonia entry into the brain leads to the upregulation of AQP4 expression in astrocytes, which represents an important mechanism underlying brain injury. Ammonia is reportedly involved in the pathogenesis of hepatic encephalopathy by regulating astrocytic AQP4 expression in the brain [28]. Zhu DD and colleagues found that AQP4 aggravates cognitive impairment in SEA by inhibiting Nav1.6-mediated astrocyte autophagy [11]. In this study, we found that ammonia entering the brain increased the expression of AQP4 in astrocytes in a mouse model of CLP. However, the potential mechanism by which AQP4 causes brain injury in this model remains unclear and requires further exploration in future research.

Limitations of our study including (1) healthy rodent animals do not represent the patients; (2) the CLP model was used in the SAE model of mice, which showed abdominal infection, and the infection sites of SAE patients in clinical practice often included the brain, lungs, abdomen, bloodstream infection and other sites,

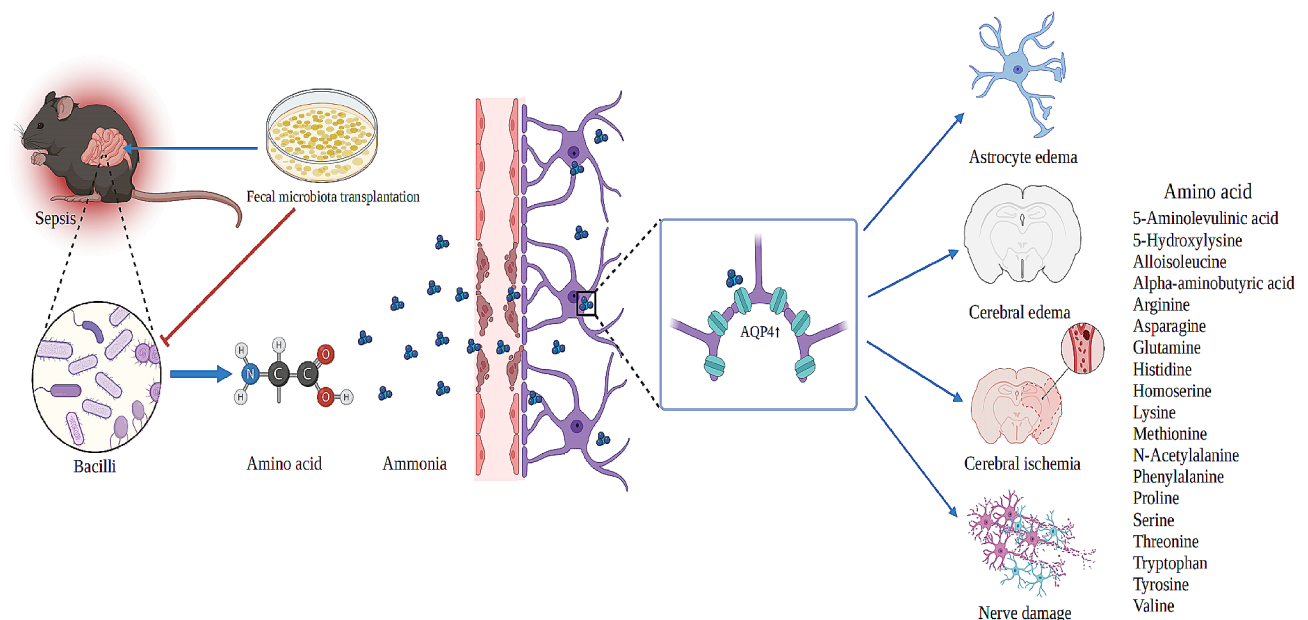


Fig. 8 A diagram of the mechanism of NHH leads to SAE. After sepsis, ammonia-producing *Bacilli* increase in the intestine, promoting the breakdown of amino acids, ammonia increases, ammonia enters the brain and aggregates in astrocytes, up-regulating the expression of astrocyte hydration protein AQP4, resulting in astrocyte activation, edema, promoting cerebral edema, cerebral ischemia, and nerve damage, leads to the occurrence of SAE

therefore, the results of this study may be more relevant to those of patients with SAE with abdominal infection in the clinic. (3) clinical relevance including the fluid resuscitation, antibiotics, vasopressor and source control in this model were not reflected, therefore, the results of this study may be biased against patients with SAE in clinical practice. In this study, we wanted to observe the effect of CLP on intestinal microbial species, but, antibiotics would a significant effect intestinal microbial species [33], therefore in this study did not use antibiotic refer to other literature related to SAE [11, 34]. (4) the changes in ammonia levels and imaging in CLP were not dynamically monitored and observed in the long term.

In summary, the disturbance of the intestinal flora after sepsis, characterized by an increase in urease-producing *bacilli*, leads to increased amino acid metabolism and ammonia production. These changes result in the upregulation of AQP4 levels in astrocytes, facilitating the entry of ammonia into the brain. Consequently, CLP mice exhibit cerebral edema, impaired structural integrity of nerve fibers, neuronal cell damage, and cognitive dysfunction, potentially representing an underlying mechanism for the occurrence of SAE. This study provides new insights into the pathological mechanisms and potential new drug targets for the treatment of SAE.

Materials and methods

Animal

The experimental procedures and animal care protocols were approved by the Committee on Ethical Use of Animals of Tianjin Medical University General Hospital. The experimental procedures followed the National Institutes of Health Guidelines for the Care and Use of Laboratory Animals. Male C57BL/6J mice, aged 8–10 weeks and weighing 20–25 g, were obtained from the Specific Pathogen-Free (SPF) Model Animal Center of the Military Medical Science Academy in Beijing, China. The mice were categorized into control, sham, CLP, and CLP+FMT groups.

CLP model

The experiment utilized the classical CLP model [29]. Briefly, after administering 2% isoflurane anesthesia and disinfecting the skin, a 1-cm incision was made along the abdominal midline to reveal the cecum. The cecum ligation was about 50% ligated between the distal pole and base, 21G needle size was used to passed through the cecum, to induce moderate sepsis. The incision was closed using a sterile 6–0 silk suture. Mice subjected to the sham operation had their cecum exposed in the same manner as those subjected to CLP, but the cecum was neither ligated nor punctured. The mice in the control group did not undergo surgery. On the day of surgery, fresh FMT was prepared by collecting the cecal contents

from healthy mice. On postoperative days one, two, and three, the selected CLP group of mice was administered 2 mL of FMT via rectal enema using a blunt vein irrigation cannula. The FMT protocol was based on the study of Kim et al. [20].

Genomic DNA extraction

Genomic DNA was extracted from the samples using an OMEGA Soil DNA Kit (D5625-01) (Omega Bio-Tek, Norcross, GA, USA). The selected V3-V4 variable region was amplified by PCR using specific primers with barcodes and high-fidelity DNA polymerase. The PCR products were detected by 2% agarose gel electrophoresis, and the fragments of interest were recollected using the Quant-IT Pico Green dsDNA Assay Kit. The PCR-amplified recovered products were assayed and quantified using a microplate reader (BioTek, FLx800) and a fluorescence quantitative system. Library-building reagents were obtained using Illumina TruSeq Nano DNA LT Library Prep Kit Box. Quality assessment of the built library was performed using a Bioanalyzer 2100 and Promega Quant Fluor.

16 S rDNA processing and analysis

The 16 S analysis uses the Silva (version138) database for species comparison and annotation. Qiime2 software was used to calculate the α β diversity indices. The analysis included the Wilcoxon rank sum test for assessing differences in α diversity (Shannon, Simpson, Chao 1) and β diversity (based on Weighted Unifrac and Unweighted U distances). Differences in community composition were analyzed using principal coordinate analysis (PCoA) or PCA.

LEfSe (LDA Effect Siz) analysis was conducted to identify species significantly impacting the differentiation of samples between groups. STAMP difference analysis was used to compare the abundance of species and the differential species functions between two sets of samples (Wilcox test analysis) or multiple sets of samples (Kruskal–Wallis test analysis). Piecrust software was used to analyze functional differences between different groups by comparing species composition information obtained from 16 S sequencing data, including KEGG and COG.

LC/MS untargeted metabolomics analysis

Following sample pretreatment, metabolite analysis was conducted using a UHPLC system (1290 Infinity LC, Agilent Technologies) combined with a QTRAP MS instrument (6500, Scitex) at Shanghai Applied Protein Technology Co., Ltd. The analytes were separated using HILIC and C18 columns in UPLC with specific column specifications (HILIC: Waters UPLC BEH Amide column, 2.1 mm \times 100 mm, 1.7 μ m; C18: Waters UPLC BEH C18-2.1 \times 100 mm, 1.7 μ m). MultiQuanta was used

for quantitative data processing. The processed data were uploaded to SIMCA-P (version 14.1, Umetrics, Umea, Sweden) for multivariate data analysis, which included Pareto-scaled principal component analysis (PCA) and other analyses.

Magnetic resonance imaging (MRI)

MRI of each group of mice was conducted using a 9.4T magnetic resonance small animal scanner (Bruker Biospin, Germany) at Tianjin Medical University General Hospital. In this experiment, MRI techniques, including T2-weighted imaging, ASL, TDI, and 1 H-MRS, were used to observe changes in cerebral edema, cerebral blood flow, nerve fiber integrity, and metabolites in each group of mice.

T2-weighted imaging

The Parameter settings for T2-weighted imaging (T2WI) were as follows: repetition time (TR)/echo time (TE)=4808/33 ms, field of view (FOV)= 20×20 mm², slice thickness=0.5 mm, number of averages (NA)=2, and slices=50.

1 H-MRS

The parameter settings for 1 H-MRS were as follows: RT/TE=1500/16.5 ms, averages=256, target voxel of interest, $4 \times 1 \times 2$ mm³. Data analyses were performed using the Bruker Para Vision 360 and Mestre Nova software (V12.0.0, Mestre Lab Research, Spain). The process of analyzing the metabolites used Cr as a standard reference.

ASL

The parameter settings for 1 H-MRS were as follows: RT/TE=4808/33 ms, FOV= 20×20 mm², image size= 128×128 , and slice=1. The ASL perfusion image was obtained using Bruker Para Vision 360 software.

DTI

The DTI parameter settings include TR of 3,000 ms, TE of 19.6 ms, 85 gradient directions, diffusion gradient on time of 4 ms, FOV= 20×20 mm², 0.5 mm slice thickness, and a 256×256 matrix. DTI images were analyzed using ParaVision 360 V3.0 software (Bruker Biospin, Germany) and DSI Studio.

HE staining

Samples from the ileum region were taken for histopathology, while the liver tissue was placed in neutral buffered formalin for fixation, with a slice thickness of 4 μ m. Paraffin sections were then deparaffinized in water stained with Harris hematoxylin for 5–10 min for nuclear staining, followed by staining with eosin staining solution for 1–3 min for cytoplasmic staining using

a dehydrated transparent mount. Intestinal villus length and crypt depth and liver tissue were measured from photomicrographs captured with an OLYMPUS eclipse inverted Microscope (OLYMPUS CKX43-LP) using image software.

Nissl staining

After routine treatment in paraffin, Sect. (8 μ m) were obtained using a microtome (Leica Histoscore MULTICUT). Paraffin sections were then dewaxed to water. Subsequently, they were stained with methylene blue staining solution for 10 min, differentiated in Nicholas differentiation solution, and processed in ammonium molybdate solution for 1 min. Following this, sections were dehydrated and transparently sealed. Observation and photography were conducted using a panoramic scanner (Panoramic Scan).

BBB permeability

The four groups of mice were injected with 4% Evans blue (EB; 2 mL/kg, Aladdin) through their tail veins. After 3 h, the mouse brain was removed, and the tissue was cut and homogenized in an ice water bath at 1000 g. The homogenate was then centrifuged for 15 min, and 750 μ L of the supernatant was collected. Acetone was added to the supernatant in a ratio of supernatant to acetone=3:7, followed by incubation at room temperature for 24 h. Thereafter, the mixture was centrifuged at 2000 g for 15 min, and the supernatant was collected. The absorbance value of both the standard and the sample was read at 620 nm using a microplate reader, and the EB concentration was calculated accordingly.

ELISA

Blood and hippocampal tissue samples were collected from each mouse centrifuged at 3000 rpm for 10 min. Serum and hippocampal tissue samples were collected according to weight (mg) to volume (mL) ratio of 1:9, with the corresponding amount of normal saline added. Grinding beads were introduced, and the samples were thoroughly ground in a high-speed and low-temperature tissue grinder. Subsequently, centrifugation at 3000 rpm for 10 min was performed, and the supernatant was immediately tested following the instructions provided for the ammonia (A086-1-1, 202,305) and glutamine (F30107-A, 202,307) assays.

Biochemical testing

After administering anesthesia, about 0.8 ml of blood from blood vessels is extracted from the heart, and the supernatant was obtained by centrifugation at 3000 rpm for 15 min at room temperature. Serum was used to measure liver function levels in mice. Alanine aminotransferase, aspartate aminotransferase, and total bilirubin levels

were measured using an automatic biochemical analyzer (XN-530, Sysmex). Quality control testing is performed prior to the application of automatic biochemical analyzer. After the application of automatic biochemical analyzer quality control test is passed, the prepared samples are sampled for test, in this process, the machine takes about 25 μ L sample. After interrupting sampler mode, perform sample analysis. When analysis of the sample is completed, close the sampler cover and press the mode switch.

Morris water maze (MWM)

The cognitive dysfunction test was conducted using the MWM [30, 31]. The apparatus had a diameter of 120 cm and a height of 45 cm, with the water temperature maintained at 20 ± 2 °C. The pool was divided into four quadrants of equal area, and the platform was placed at the center of the target quadrant. Each mouse in all groups was trained for four consecutive days (9–12 days after CLP) to find the platform and reach a plateau. The time taken by the mice to reach the platform was separately recorded after they entered the water in each quadrant, serving as the latency period. If the mouse failed to find the platform within 60 s, the experimenter guided it to the platform and allowed it to remain there for 10 s, with an escape latency of 60 s. In the probe test (13 days after CLP), mice were placed in water opposite the target quadrant, and the number of times they passed through the original plateau area within 60 s was recorded, along with the time spent in the target quadrant.

(Novel object recognition) NOR

The NOR was used to evaluate the cognitive function of exploring new object abilities [32]. Before the experiment, the mouse was gently placed in a square box ($50 \times 50 \times 40$ cm³) for 3 min to acclimate to the environment. The box was equipped with a camera directly above it, connected to the Super Maze Animal Behavior Video Analysis System (Xinruan Information Technology Ltd, Shanghai, China).

Subsequently, the mice were randomly placed in the center of the arena, where two identical objects were explored for 5 min each (day 7 after CLP). On day 8 after CLP, the two familiar objects were replaced with a novel object, and the mice were allowed to explore for 5 min. The novel object and discrimination index [(time spent exploring the novel object/time spent exploring the two objects) \times 100%] were recorded and analyzed.

QT-PCR

Hippocampal samples were collected from the brain tissue, and cell experiments were performed using C8-D1A (mouse cerebellar astrocytes)/CL-0506. TRIzol lysate was added, and total RNA was extracted. RNA

was synthesized using a ReverTra Ace qPCR RT Kit to synthesize cDNA. A denaturation buffer was added to the cell sample to induce cell lysis, followed by RNA extraction, precipitation, washing, solubilization, and assessment of RNA integrity. Real-time fluorescence quantification PCR was performed using specific primers. For the gene of interest, the upstream primers of GFAP were 5'- AACAACCTGGCTGCGTATAGAC -3'; and the downstream primers of GFAP: 5'- ATCTCCTCC TCCAGCGATTCAA -3'. Similarly, for AQP4, upstream primers were 5'- GCATCGCTAAGTCCGTCTTCT -3'; and the downstream primers were 5'- GAGGTGTGACC AGGTAGAGGAT -3'. For B-actin, the upstream primers were 5'- GTACTCTGTGTGGATCGGTGG -3'; and the downstream primers were 5'- GCAGCTCAGTAACAGT CCG -3'. The PCR protocol included pre-denaturation at 95 °C for 10 min, followed by denaturation at 95 °C for 15 s, annealing at 62 °C with elongation for 1 min, and a total of 40 cycles.

Immunofluorescence

Briefly, the brain samples were fixed overnight in 4% paraformaldehyde and subjected to immunofluorescence staining. The astrocytes were pre-treated with NH₄Cl (Chemuza, 12125-02-9) or TGN020 (Selleck, S0158). Primary astrocytes were then removed from the cell incubator and fixed in 4% paraformaldehyde after washing, followed by permeabilization in 0.3% TX-100 and blocking with 2% bovine serum albumin (BSA). The cells were treated with primary antibodies, including mouse anti-GFAP (1:300, Wuhan Mitaka, 60190-1-Ig), rabbit anti-AQP4 (1:300, Wuhan Mitaka, 16473-1-AP) overnight at 4 °C. Subsequently, the cells were then incubated with secondary antibodies: goat anti-rabbit IgG/TRITC (1:100; Nakasugi Golden Bridge, ZF-0316) and goat anti-mouse IgG/FITC (1:100; Nakasugi Golden Bridge, ZF-0312). All images were acquired using a panoramic scanner (3DHISTECH Panoramic Scan). Positive fluorescence staining was calculated using image software.

Western blot analysis

Brain tissue and astrocyte samples were homogenized in RIPA buffer to extract the proteins. Different groups of brain tissues and astrocytes were treated with different drugs. The primary antibodies used included mouse anti-GFAP (1:10000, Wuhan Mitaka, 60190-1-Ig), rabbit anti-AQP4 (1:15000, Wuhan Mitaka, 16473-1-AP), Mouse Anti- β -tubulin (1:2000, Nakasugi Kanabashi, TA-10). The sample-loaded membranes were incubated overnight at 4 °C and then, post 8–12 h of incubation, treated with secondary antibody, Goat Anti-Rabbit IgG(1:5000, Nakasugi Golden Bridge, ZB-2301), and Goat Anti-MOUSE IgG(1:5000, Nakasugi Golden Bridge, ZB-2301). A gel

imaging analysis system (Beijing Saizhi, Champchemi 610 plus) was used to detect band signals.

Astrocytes CCK8 assay

Astrocyte viability was determined using a CCK8 kit (BS350A, Biosharp). The cell suspension was seeded in a 96-well plate with 100 μ L per well, containing 5,000 cells per well. Subsequently, 10 μ L of CCK8 solution was added to each well, and the plate was further incubated in the cell culture incubator for 1–4 h.

Astrocyte culture

The brain tissues of C57BL/6J mice were extracted and digested with 0.125% trypsin in Dulbecco's modified Eagle's medium (DMEM) in a cell culture incubator. DMEM containing 10% fetal bovine serum (FBS) was used to terminate the digestion. Single cells were seeded at a density of 1×10^6 cells/well in a 24-well culture plate pre-coated with polylysine, with a density of approximately 4 cm^{-2} . After 72 h, the medium was replaced with a fresh, complete medium, and the cells were cultured for approximately 7 days to achieve 90% cell growth coverage. The plate was then spun at 260 rpm (24 h, 37 °C) to collect purified astrocytes [11].

Statistical analysis

All data were expressed as the mean \pm standard deviation (SD). GraphPad Prism 10.0.2 software (San Diego, CA, USA) was used for data analysis. Statistical significance was assessed using Student's *t*-test, Mann–Whitney *U* test, ANOVA for multiple comparisons, two-way ANOVA with Tukey's post hoc test, and one-way ANOVA with Tukey's post hoc test. $p < 0.05$ was considered statistically significant.

Abbreviations

SAE	Sepsis-associated encephalopathy
NHH	Non-hepatic hyperammonemia
CLP	Cecal ligation and perforation
ASL	Arterial spin labeling
DTI	Diffusion Tensor Imaging
1H-MRS	Proton magnetic resonance spectroscopy
AQP4	Aquaporin4channel
GFAP	Glial fibrillary acidic protein
KEGG	Kyoto encyclopedia of genes and genomes
GO	Gene ontology
PCoA	Principal coordinate analysis
LEFSe	LDA effect size
FA	Fractional anisotropy
AD	Axial diffusion
RD	Radical diffusion
MD	Mean Diffusivity
Glu	Glutamate
Cr	Creatine
NAA	N-acetylaspartate
Glx	Glutamate + glutamine, T2WI: T2 weighted image

Supplementary Information

The online version contains supplementary material available at <https://doi.org/10.1186/s12974-024-03135-2>.

Supplementary Material 1

Supplementary Material 2

Acknowledgements

We would like to thank to "Zhongke New Life Biotechnology Co., Ltd." for providing intestinal microbiota and metabolomics analysis and department of imaging of General Hospital of Tianjin Medical University for providing mice fMRI and thank Editage (www.editage.cn) for English language editing.

Author contributions

L.N.Z. and K.L.X., Y.L. contributed to the conception and design of the project, they played a major role in performing experiments and analyzing the data, as well as writing the initial draft of the manuscript. L.N.Z., Z.Z., H.N.W., J.Y.Z., P.W., N.N.Z., F.Y., Z.W.W., Y.Y.W., H.Y.Z., H.B.L., Z.F.H., H.S., Z.Y.W., and F.H. S contributed to conducting the experiments. K.L.X., and Y.L. modified the language. All authors read and approved the final version of the manuscript.

Funding

This work was supported by the grant from the Natural Science Foundation of Inner Mongolia Autonomous Region (serial number 2022MS08002); Tianjin Municipal Health Commission (serial number TJWJ2023QN007); National Natural Science Foundation of China (82302413).

Data availability

No datasets were generated or analysed during the current study.

Declarations

Ethical approval

All animal experiments were carried out according to the Institutional Animal Care and Use Committee guidelines of the NIH, USA, and approved by the Institutional Ethics Committee of Tianjin Medical University General Hospital.

Competing interests

The authors declare no competing interests.

Received: 26 March 2024 / Accepted: 20 May 2024

Published online: 27 May 2024

References

1. Iwashyna TJ, Ely EW, Smith DM, Langa KM. Long-term cognitive impairment and functional disability among survivors of severe Sepsis. *JAMA*. 2010;304(16):1787.
2. Djillali A, Tarek S. Cognitive decline after sepsis. *Lancet Respiratory Med*. 2015;3(1):61–9.
3. Eidelman LA, Putterman D, Putterman C, Sprung CL. The spectrum of septic encephalopathy. Definitions, etiologies, and mortalities. *JAMA*. 1996;275(6):470–3.
4. Safadi R, Rahimi RS, Thabut D, Bajaj JS, Ram Bhamidimarri K, Pyrsopoulos N, Potthoff A, Bukofzer S, Wang L, Jamil K, Devarakonda KR. Pharmacokinetics/ pharmacodynamics of L-ornithine phenylacetate in overt hepatic encephalopathy and the effect of plasma ammonia concentration reduction on clinical outcomes. *Clin Transl Sci*. 2022;15(6):1449–59.
5. Li Y, Yao Z, Li Y, Yang Z, Li M, Chen Z, Liu S, Gong J, Huang L, Xu P, Li Y, Li H, Liu X, Zhang L, Zhang G, Wang H. Prognostic value of serum ammonia in critical patients with non-hepatic disease: a prospective, observational, multicenter study. *J Transl Int Med*. 2022;11(4):401–9.
6. Pandey S, Tun MM, Htet SY, Chhetri B, K C N. Recurrent Non-cirrhotic Hyperammonemic Encephalopathy Due to Complicated Urinary Tract Infection: A Case Report. *Cureus*. 2023, 15(5):e39579.

7. Sakusic A, Sabov M, McCambridge AJ, Rabinstein AA, Singh TD, Mukesh K, Kashani KB, Cook D, Gajic O. Features of adult hyperammonemia not due to liver failure in the ICU. *Crit Care Med*. 2018;46(9):e897–903.
8. Wang P, Yan J, Shi Q, Yang F, Li X, Shen Y, Liu H, Xie K, Zhao L. Relationship between Nonhepatic Serum Ammonia Levels and Sepsis-Associated Encephalopathy: A Retrospective Cohort Study. *Emerg Med Int*. 2023; 2023:6676033.
9. Zhao L, Li Y, Wang Y, Ge Z, Zhu H, Zhou X, Li Y. Non-hepatic hyperammonemia: a potential therapeutic target for Sepsis-associated Encephalopathy. *CNS Neurol Disord Drug Targets*. 2022;21(9):738–51.
10. Dickson RP, Singer BH, Newstead MW, Falkowski NR, Erb-Downward JR, Standiford TJ, Huffnagle GB. Enrichment of the lung microbiome with gut bacteria in sepsis and the acute respiratory distress syndrome. *Nat Microbiol*. 2016;18(110):16113.
11. Zhu DD, Huang YL, Guo SY, Li N, Yang XW, Sui AR, Wu Q, Zhang Y, Kong Y, Li QF, Zhang T, Zheng WF, Li AP, Yu J, Ma TH, Li S. AQP4 aggravates cognitive impairment in Sepsis-Associated Encephalopathy through Inhibiting Nav 1.6-Mediated astrocyte autophagy. *Adv Sci (Weinh)*. 2023;10(14):e2205862.
12. Ribas GS, Lopes FF, Deon M, Vargas CR. Hyperammonemia in inherited metabolic diseases. *Cell Mol Neurobiol*. 2022;42(8):2593–610.
13. Rump K, Adamzik M. Function of aquaporins in sepsis: a systematic review. *Cell Bioscience*. 2018;8(1):10–2018.
14. Zhao L, Gao Y, Guo S, Lu X, Yu S, Ge Z, Zhu H, Li Y. Prognosis of patients with Sepsis and non-hepatic hyperammonemia: a Cohort Study. *Med Sci Monit*. 2020;26:e928573.
15. Xie K, Fu W, Xing W, Li A, Chen H, Han H, Yu Y, Wang G. Combination therapy with molecular hydrogen and hyperoxia in a murine model of polymicrobial sepsis. *Shock*. 2012;38(6):656–63.
16. Halpin LE, Northrop NA, Yamamoto BK. Ammonia mediates methamphetamine-induced increases in glutamate and excitotoxicity. *Neuropsychopharmacol Official Publication Am Coll Neuropsychopharmacol*. 2014;39(4):1031–8.
17. Yao ZP, Li Y, Liu Y, Wang HL. Relationship between the incidence of non-hepatic hyperammonemia and the prognosis of patients in the intensive care unit. *World J Gastroenterol*. 2020;26(45):7222–31.
18. etaj N, Stazi GV, Marini MC, Garotto G, Busso D, Scarcia S, Caravella I, Macchione M, De Angelis G, Di Lorenzo R, Carucci A, Capone A, Antinori A, Palmieri F, D'Offizi G, Taglietti F, Ianniello S, Campioni P, Vaia F, Nicastrì E, Girardi E, Marchioni L. On Behalf of Icu Covid-Study Group. Epidemiology, clinical presentation and treatment of non-hepatic hyperammonemia in ICU COVID-19 patients. *J Clin Med*. 2022;11(9):2592.
19. Hu Q, Ren H, Li G, Wang D, Zhou Q, Wu J, Zheng J, Huang J, Slade DA, Wu X, Ren J. STING-mediated intestinal barrier dysfunction contributes to lethal sepsis. *EBioMedicine*. 2019;41:497–508.
20. Kim SM, DeFazio JR, Hoyoju SK, Sangani K, Keskey R, Krezalek MA, Khodarev NN, Sangwan N, Christley S, Harris KG, Malik A, Zaborin A, Bouziat R, Ranoa DR, Wiegnerinck M, Ernest JD, Shakhsheer BA, Fleming ID, Weichselbaum RR, Antonopoulos DA, Gilbert JA, Barreiro LB, Zaborina O, Jabri B, Alverdy JC. Fecal microbiota transplant rescues mice from human pathogen mediated sepsis by restoring systemic immunity. *Nat Commun*. 2020;11(1):2354.
21. Wang P, Wu PF, Wang HJ, Liao F, Wang F, Chen JG. Gut microbiome-derived ammonia modulates stress vulnerability in the host. *Nat Metab*. 2023;5(11):1986–2001.
22. Achal V, Pan X. Characterization of Urease and carbonic anhydrase producing Bacteria and their role in Calcite Precipitation. *Curr Microbiol*. 2011;62(3):894–902.
23. Giridharan VV, Generoso JS, Lence L, Candiotto G, Streck E, Petronilho F, Pillai A, Sharshar T, Dal-Pizzol F, Baricello T. A crosstalk between gut and brain in sepsis-induced cognitive decline. *J Neuroinflammation*. 2022;19(1):114.
24. Zhang H, Xu J, Wu Q, Fang H, Shao X, Ouyang X, He Z, Deng Y, Chen C. Gut microbiota mediates the susceptibility of mice to Sepsis-Associated Encephalopathy by Butyric Acid. *J Inflamm Res*. 2022;15:2103–19.
25. Görg B, Karababa A, Shafiqullina A, Bidmon HJ, Häussinger D. Ammonia-induced senescence in cultured rat astrocytes and in human cerebral cortex in hepatic encephalopathy. *Glia*. 2015;63(1):37–50.
26. Rangroo Thrane V, Thrane AS, Wang F, Cotrina ML, Smith NA, Chen M, Xu Q, Kang N, Fujita T, Nagelhus EA, Nedergaard M. Ammonia triggers neuronal disinhibition and seizures by impairing astrocyte potassium buffering. *Nat Med*. 2013;19(12):1643–8.
27. Kitchen P, Salman MM, Halsey AM, Clarke-Bland C, MacDonald JA, Ishida H, Vogel HJ, Almutiri S, Logan A, Kreida S, Al-Jubair T, Winkel Missel J, Gourdon P, Törnroth-Horsefield S, Conner MT, Ahmed Z, Conner AC, Bill RM. Targeting Aquaporin-4 subcellular localization to treat Central Nervous System Edema. *Cell*. 2020;181(4):784–e79919.
28. Chastre A, Jiang W, Desjardins P, Butterworth RF. Ammonia and proinflammatory cytokines modify expression of genes coding for astrocytic proteins implicated in brain edema in acute liver failure. *Metab Brain Dis*. 2010;25(1):17–21.
29. Rittirsch D, Huber-Lang MS, Flierl MA, Ward PA. Immunodesign of experimental sepsis by cecal ligation and puncture. *Nat Protoc*. 2009;4(1):31–6.
30. Silva AYO, Amorim EA, Barbosa-Silva MC, Lima MN, Oliveira HA, Granja MG, Oliveira KS, Fagundes PM, Neris RLS, Campos RMP, Moraes CA, Vallochi AL, Rocco PRM, Bozza FA, Castro-Faria-Neto HC, Maron-Gutierrez T. Mesenchymal stromal cells protect the blood-brain barrier, reduce astrogliosis, and prevent cognitive and behavioral alterations in surviving septic mice. *Crit Care Med*. 2020;48(4):e290–8.
31. Vorhees CV, Williams MT. Morris water maze: procedures for assessing spatial and related forms of learning and memory. *Nat Protoc*. 2006;1(2):848–58. (2006).
32. Bevins RA, Besheer J. Object recognition in rats and mice: a one-trial non-matching-to-sample learning task to study 'recognition memory'. *Nat Protoc*. 2006;1(3):1306–11.
33. Lange K, Buerger M, Stallmach A, Bruns T. Effects of Antibiotics on Gut Microbiota. *Dig Dis*. 2016;34(3):260–8.
34. Li HR, Liu Q, Zhu CL, Sun XY, Sun CY, Yu CM, Li P, Deng XM, Wang JF. β -Nicotinamide mononucleotide activates NAD⁺/SIRT1 pathway and attenuates inflammatory and oxidative responses in the hippocampus regions of septic mice. *Redox Biol*. 2023;63:102745.
35. Chu J, Li H, Yuan Z, Zhou W, Yu Y, Yu Y. Acetaminophen impairs ferroptosis in the hippocampus of septic mice by regulating glutathione peroxidase 4 and ferroptosis suppressor protein 1 pathways. *Brain Behav*. 2023;13(8):e3145.

Publisher's Note

Springer Nature remains neutral with regard to jurisdictional claims in published maps and institutional affiliations.